ACS OMEGA

http://pubs.acs.org/journal/acsodf

Article

Cu and Zn Bimetallic Co-Modified H-MOR Catalyst for Direct Oxidation of Low-Concentration Methane to Methanol

Yan Fu, Cunshuo Li, Shengxin An, Wenzhi Li,* and Liang Yuan

Cite This: *ACS Omega* 2023, 8, 27179−27189

Read Online

ACCESS | Metrics & More | Article Recommendations | Supporting Information

ABSTRACT: The direct oxidation of low-concentration methane to value-added chemicals can not only reduce carbon emission but also provide an alternative production route for fossil fuels. Herein, we proposed a novel catalyst for the direct oxidation of low-concentration methane to methanol via the impregnation method, which selected copper and zinc as co-modifiers to modify the MOR catalyst. The highest methanol yield of 71.35 μmol·g_{cat}^{-1}·h^{-1} was obtained over a bimetallic $Cu_{0.5}Zn_{0.35}$-MOR catalyst. The catalyst retained good activity after three cycles of testing experiments, indicating good recyclability. Based on the results of performance tests and characterization studies, it was confirmed that Cu species bound to the zeolite framework were the main active sites for methane oxidation. The introduction of Zn decreased the generation of the octahedrally coordinated extra-framework aluminum, which promoted the dispersion of Cu within the zeolite framework. In other words, more tetrahedrally coordinated FAl-stabilized Cu species were presented in our CuZn-MOR catalyst system in comparison to the monometallic Cu-MOR catalyst. Benefiting from the aforementioned modification, the agglomerative sintering of the metal during the reaction was effectively prevented. This work may provide a feasible guide for the future optimization of Cu-based catalysts designed for the selective oxidation of methane.

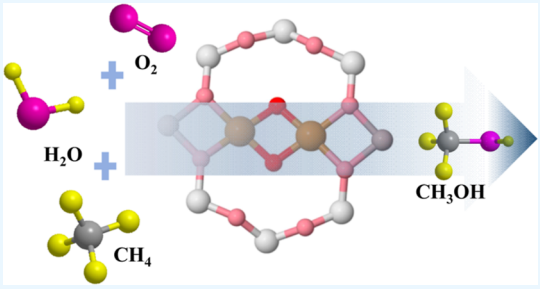

1. INTRODUCTION

Methane, the main component of natural gas, is widely distributed in abundant resources such as natural gas, shale gas, and coalbed methane.[1−3] In addition, methane also is the most promising energy carrier and raw material for chemicals because of its large reserves and relatively low price.[4,5] Large amounts of low-concentration methane (the methane content in mixtures is less than 30 vol %) were inevitably generated during resource extraction, especially in coalbed methane. The utilization of low-concentration methane has remained a hot area of research internationally. In addition, most of the resource extraction sites were located in remote areas, and low-concentration methane was largely disposed of by direct emission or in situ combustion due to storage and transportation constraints.[6−9] Since the greenhouse effect of methane was 25 times greater than that of carbon dioxide, these disposal methods both increased environmental pollution and resulted in wasted resources. Therefore, it was highly desirable to directly convert low-concentration methane into liquid chemicals that could be easily transported and stored, which would be more economical and environmentally friendly.[10,11]

In energy-intensive industrial processes, methane was first converted to syngas through reforming or partial oxidation and then to chemicals such as methanol or other hydrocarbons.[12−15] However, methane was extremely challenging to convert because of its unique molecular structure. It has a completely symmetrical tetrahedral structure, high C−H bond strength (413 kJ·mol^{-1}), negligible electron affinity, and low polarization, thus needing harsh activation conditions.[16−18] In addition, once the first C−H bond in methane was activated, the reaction intermediates and even the target products were more active and thus more prone to be over-oxidized.[19,20] In nature, enzymes convert CH_4 directly to methanol (CH_3OH) at ambient temperatures using oxygen-containing molecules such as water, oxygen, and carbon dioxide, unlike commercial processes that require the energy-intensive formation of syngas (H_2 and CO).[7] Because natural enzymes such as methane monooxygenase can selectively convert methane to methanol at normal temperature and pressure, a lot of research has been conducted on the properties of this enzyme, with a view to its application in the field of heterogeneous catalysis. The application of this bionics strategy to heterogeneous catalysts is often limited by high temperature, but some oxides and metal oxide surfaces can dissociate CH_4 at room temperature, which provides the possibility of direct conversion of CH_4 → CH_3OH.[21,22] Nevertheless, the direct conversion of methane,

Received: April 9, 2023
Accepted: July 6, 2023
Published: July 18, 2023

especially low-concentration methane, to methanol and other liquid fuels at high yields is still a huge challenge.

Zeolites were widely used in reforming, hydro-isomerization, cracking, and alkylation reactions due to its acidic surface and unique pore structure. Among them, mordenite (MOR) was a main research framework widely studied in the methane conversion reaction because of its special structure and strong loading capacity for the active site.[21,23−28] In general, active clusters are selectively stabilized in the eight-membered ring structure of this zeolite. Previous literature also confirmed the relevant role of eight-membered rings in promoting the stability and reactivity of active sites.[29,30] In particular, copper zeolite catalysts were widely used in the field of methane conversion to methanol due to its propensity to form active Cu-oxo clusters.[30−34] However, the octahedrally coordinated extra-framework aluminum (EFAl) generated during the preparation will hinder the distribution of copper by blocking the zeolite pores,[34] which will also make the copper more inclined to form agglomerates or particles on the zeolite surface, thus decreasing the atomic utilization of copper. Therefore, it is necessary to modify the catalyst to improve the dispersion of copper on the zeolite framework to enhance the catalyst activity.

Many studies have shown that an appropriate modifier can not only affect the formation and stability of catalyst active sites but also regulate the interaction between catalyst components to improve the reactivity. Priya et al. synthesized PtCu−MOR bimetallic catalyst and applied it to the formation of 1,3-propylene glycol by selective hydrolyzation of glycerol with steam in a continuous fixed-bed reactor under atmospheric pressure. The results showed that the PtCu catalyst with a small particle size and good dispersion had a porous system and strong bimetallic phase−support interaction, which finally improved the selectivity of 1,3-propylene glycol.[26] Hammond et al. confirmed that CuFe-ZSM-5 catalyst catalyzes the oxidation of methane to methanol under liquid-phase conditions, whose activity was 3 orders of magnitude higher than previously reported.[35] The research results of Yu et al. also confirmed that Cu-promoted Fe/ZSM-5 catalyst with monomeric Fe^{n+} species directly converted methane into methanol in the liquid phase and had good reactivity.[36] Furthermore, Yang et al. reported the transition metals (Zn, Cu, and Mn) and Na co-modified iron catalysts for CO_2 hydrogenation. The results demonstrated that the doping of Zn and Cu facilitated the formation of the active phase, thus promoting the reaction.[37] According to some literature reports, the strong interaction between Cu and Zn can promote the high dispersion and sintering resistance of Cu. For example, previous studies by Wang et al. showed that the Cu−ZnO interaction after activation could inhibit the sintering and stabilize the distribution of active species during the reaction.[38] Behrens et al. reported that the active site of the Cu/ZnO/Al_2O_3 catalyst was Zn-decorated Cu steps and used DFT calculations to demonstrate the Cu−ZnO synergistic effect.[39] Later, Zhang et al. proved that the Cu−ZnO−Al_2O_3 catalyst underwent in situ reconstruction during the water gas shift and CO hydrogenation reactions, forming different Cu−Zn synergistic active sites.[40] These studies indicated that the interaction between copper and zinc plays a role in enhancing the activity of the catalyst. Therefore, we speculate that this interaction could work in the direct oxidation of methane to methanol.

In this work, we synthesized a novel bimetallic CuZn−MOR catalyst via the impregnation method for the oxidation of low-concentration methane to methanol. X-ray diffraction (XRD), inductively coupled plasma (ICP), N_2-physisorption, scanning electron microscopy (SEM), transmission electron microscopy (TEM), energy-dispersive system (EDS)-mapping, hydrogen temperature program reduction (H_2-TPR), ^{27}Al MAS nuclear-magnetic-resonance (NMR), X-ray photoelectron spectroscopy (XPS), diffuse reflectance ultraviolet−visible (DR UV−Vis) spectroscopy, and CH_4-temperature program desorption (CH_4-TPD) were conducted to analyze the relevant physicochemical properties of catalysts. The results of these analyses suggested that in the CuZn−MOR catalyst, the good dispersion of Zn and Cu in the zeolite framework promoted the generation of active sites, thus enhancing the reactivity.

2. EXPERIMENTAL SECTION

2.1. Synthesis of Catalysts. *2.1.1. Materials.* The parent material H-form mordenite zeolite (Si/Al = 25) was purchased from Nankai University Catalyst Co., Ltd. of China; copper(II) acetate monohydrate ($Cu(CH_3COO)_2{\cdot}H_2O$, 99%) and zinc(II) nitrate hexahydrate ($Zn(NO_3)_2{\cdot}6H_2O$, 98%) were purchased from Sinopharm chemical reagent Co., Ltd.; methane (CH_4, 15.0 vol % in N_2) and oxygen (O_2, 21.0 vol % in N_2) were used for the catalytic performance testing. All of the chemicals described above were used directly without further treatment.

2.1.2. Synthesis of CuZn−MOR. The catalysts in this work were prepared from the corresponding metal salt precursors via the impregnation method. For the CuZn−MOR catalysts, the requisite amount of precursor solution (15 mL) was prepared by dissolving a required amount of copper(II) acetate monohydrate and zinc(II) nitrate hexahydrate in deionized water. 1.00 g H-form mordenite zeolite (Si/Al = 25) was placed in a 25 mL beaker equipped with a magnetic stirrer. After that, the precursor solution was slowly added to the mordenite powder, and then the mixed slurry was stirred at 60 °C for 12 h to fully load Cu and Zn cations. The obtained material was further dried overnight in an oven at 110 °C, followed by calcination at 550 °C with a heating ramp of 1 °C·min^{-1} for 4 h in air. Cu-MOR was synthesized using bare H-MOR treated with the same process except for the addition of Zn, while Zn-MOR was prepared without the introduction of Cu. At the end, the obtained catalyst was denoted as Cu_xZn_y−MOR (x and y refer to the ratio of the weight percentage of Cu and Zn, respectively). $Cu_{0.50}$-MOR refers to the sample with 0.50 wt % of Cu. The basic properties of all the above catalysts are shown in Table 1.

Table 1. Physicochemical Properties of the Samples

samples	S_{BET}[a]	D_{pore}[a]	V_{pore}[a]	content of metal[b]	
				Cu	Zn
H-MOR	614	3.83	0.22	n. a.	n. a.
$Cu_{0.50}$-MOR	579	3.91	0.22	0.41	n. a.
$Zn_{0.35}$-MOR	556	3.88	0.22	n. a.	0.27
$Cu_{0.5}0$ $Zn_{0.35}$-MOR	608	3.85	0.22	0.48	0.30

[a]S_{BET}—cumulative surface area ($m^2{\cdot}g^{-1}$), V_{pore}—cumulative pore volume ($cm^3{\cdot}g^{-1}$), D_{pore}—pore width (nm), obtained by N_2 physisorption results. [b]Determined by ICP−OES (wt %). n.a., not available.

https://doi.org/10.1021/acsomega.3c02388
ACS Omega 2023, 8, 27179−27189

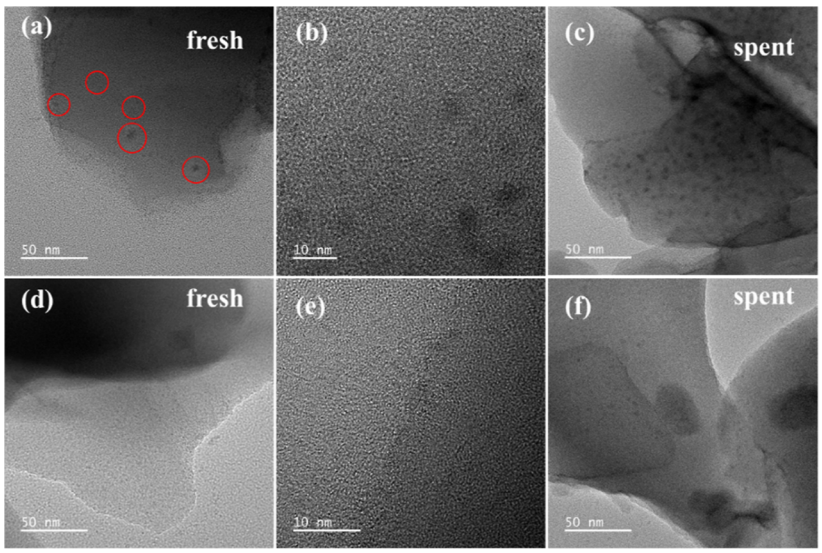

Figure 1. TEM images of fresh catalyst and the catalyst after three cycles for $Cu_{0.50}$-MOR (a−c) and (d−f) $Cu_{0.50}Zn_{0.35}$-MOR.

2.2. Characterization of Representative Samples. The physical and chemical properties of the representative samples were characterized by ICP−atomic emission spectrometry (AES), XRD, N_2-physisorption experiments, field-emission TEM, the TEM EDS elemental mapping, SEM, XPS, ^{27}Al magic-angle-spinning NMR (^{27}Al MAS NMR), H_2-TPR, CH_4-TPD, and DR UV−Vis spectroscopy. More details on the characterization procedures are provided in the Supporting Information.

2.3. Catalytic Activity Test. The activity tests of low-concentration methane conversion to methanol were carried out in a quartz fixed-bed reactor. In the case of methane conversion to methanol reaction, the 50 mg catalyst was loaded in a fixed-bed quartz reactor (inner diameter of 4 mm) and was supported by quartz wool. The flow rate of each gas was controlled by a mass flow controller (Sevenstar Instruments). The reaction temperature was monitored with a thermocouple located just above the catalyst bed. The steam was generated in a vaporizer maintained at 140 °C. The flow rate of the liquid water fed into the vaporizer was controlled with a Lead Fluid TYD01 syringe pump (Baoding Lead Fluid Technology Co., Ltd.). Notably, the gas line from the point of liquid injection to the reactor unit were all heated (T = 150 °C) by resistive heating tape to avoid condensation. Finally, the outlet gas from the reactor flows first through a cold trap (set to −3 °C) before entering a gas chromatograph (GC) for online analysis. The GC separates the products with an HP-PLOT/Q column and detects the product signal with a flame ionization detector. Detailed equipment diagram is shown in Figure S1. The yield and selectivity of the products were analyzed by calibrated GC and ^{1}H NMR (Figure S8). The CH_3OH space-time yield (STY_{CH3OH}) was computed as $N_{CH_3OH}/(M_{cat} \times T)$, where N_{CH_3OH} represented the molar amount of methanol collected in the cold trap, M_{cat} represented the mass of the catalyst, and T represented the reaction time. The selectivity of CO_2 was calculated as $S_{CO_2} = N_{CO_2}/(N_{CH_4} + N_{CO_2})$, where N_{CH_4} and N_{CO_2} represented the molar amount of CO_2 and CH_4, respectively. The methane conversion was calculated as $C_{CH_4} = (1 - N_{outlet}/N_{inlet}) \times 100\%$.

2.3.1. Repeat the cycle test. When the activity test experiment was completed, the reaction bed was cooled naturally to room temperature, and then the previous experimental procedure was repeated. Each repetition is called a cycle and is repeated three times in total.

3. RESULTS AND DISCUSSION

3.1. Morphological and Structural Characterization. The morphology of the synthesized catalysts was scrutinized with SEM and TEM. The SEM images of the bare H-MOR and $Cu_{0.50}Zn_{0.35}$-MOR catalyst are presented in Figure S2, in which the modified zeolite did not show a distinct surface or morphology compared with the bare H-MOR sample. This phenomenon indicated that the structure and morphology of the parent zeolite were not significantly damaged after impregnation and calcination. In addition, the SEM images showed that no metal particles were observed, indicating that Cu and Zn were well dispersed on the zeolite. Moreover, the TEM images of fresh $Cu_{0.50}$-MOR and $Cu_{0.50}Zn_{0.35}$-MOR catalysts are displayed in Figure 1a,b,d,e, respectively. It can be observed that some metal particles were present on the $Cu_{0.50}$-MOR catalyst, while no obvious particles were found on the $Cu_{0.50}Zn_{0.35}$-MOR catalyst. In addition, the EDS-mapping results (Figure S4) showed that the presence of copper was always accompanied by the presence of zinc. All these results indicated that both Cu and Zn metals may be uniformly dispersed in the MOR.[23,41,42] Furthermore, the TEM images of the $Cu_{0.50}$-MOR and $Cu_{0.50}Zn_{0.35}$-MOR catalysts after three cycles are also shown in Figure 1c,f, respectively. After three cycles of heating and cooling of the reaction, metal sintering agglomeration occurred to varying degrees in both catalysts. More pronounced metal particles appeared in the $Cu_{0.50}$-MOR catalyst than in the fresh catalyst, in contrast to that observed in the $Cu_{0.50}Zn_{0.35}$-MOR catalyst where only a small amount of metal agglomerates was observed. This phenomenon illustrated the better metal dispersion in the $Cu_{0.50}Zn_{0.35}$-MOR catalyst. Moreover, it was a good proof that the introduction of Zn did promote the dispersion of copper on zeolites and hindered the formation of metal agglomerates.

As shown in Figure 2, the XRD pattern of the modified mordenite catalysts revealed characteristic peaks similar to the

https://doi.org/10.1021/acsomega.3c02388
ACS Omega 2023, 8, 27179−27189

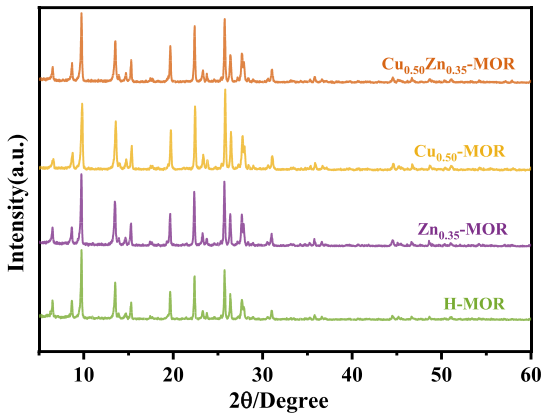

Figure 2. XRD patterns of various catalysts by impregnation methods.

bare H-MOR diffraction peak at 2θ = 9.76, 13.52, 19.70, 22.42, 25.73, 26.44, and 27.64°.[23,33,42] They were the typical signs of well-crystallized mordenite zeolite. In addition, all of the samples presented similar crystallinity, and no significant differences were observed in the mordenite structure after metal impregnation. The results showed that the structure and crystallinity of the mordenite were retained, and standard diffraction peaks corresponding to CuO phases (JCPDS file no. 80-1917) or Cu_2O phases (JCPDS file no. 78-2076) were not observed in XRD patterns, which could be attributed to two possible reasons: (i) copper and zinc contents were too low (the actual loading of Cu and Zn measured by ICP−AES were 0.48 and 0.30 wt %, respectively, Table 1) on the $Cu_{0.50}Zn_{0.35}$-MOR catalyst, and (ii) these metal species were highly dispersed throughout the mordenite framework and Cu-based nanoparticles, if any, were smaller than ∼3 nm.

The specific surface area of the CuZn−MOR catalysts was obtained by nitrogen adsorption−desorption experiments. As shown in Figure 3, the hysteresis loops were displayed in the

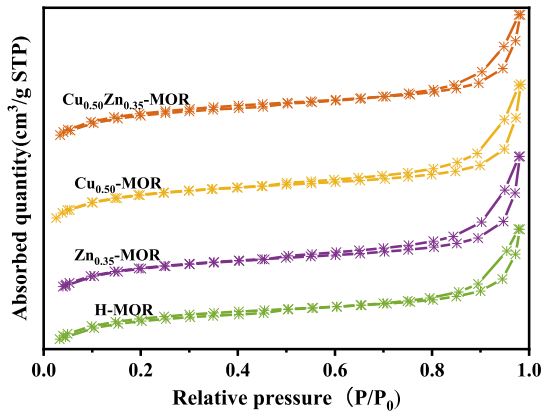

Figure 3. Nitrogen adsorption−desorption isotherms of various catalysts by impregnation methods.

adsorption isotherm curves, which conform to the type IV adsorption isotherm of IUPAC classification,[43] confirming the presence of a mesopore structure in the catalysts. Compared with H-MOR, a decrease in the Brunauer−Emmett−Teller (BET) surface area of the modified catalyst was observed, which can be explained by pore filling by modified metals (Table 1).[44] Among them, the $Zn_{0.35}$-MOR and $Cu_{0.50}$-MOR catalysts showed the largest decrease in S_{BET} and an increase in D_{pore}, suggesting that some of the micropores in the zeolite were filled. However, the minimum decrease of S_{BET} and a smaller change of D_{pore} in the $Cu_{0.50}Zn_{0.35}$-MOR catalyst, together with the TEM results above, can further demonstrate that the introduction of Zn promoted the dispersion of Cu in the MOR and thus decreased pore plugging. In addition, as depicted in Table 1, the pore size distribution of the catalysts also remained unchanged obviously, indicating that the metal loading did not have a great influence on the pore volume of H-MOR. These results are consistent with the XRD and morphology analysis.

3.2. Chemical Properties. In the process of methane conversion reaction, the adsorption of the reactant by the catalyst had a profound influence on the reaction. In order to elucidate the effect of Zn doping on the adsorption behavior of methane on the corresponding catalyst samples, CH_4 temperature-programmed desorption (CH_4-TPD) experiments were performed in a conventional flow system.[45] It can be seen from Figure 4 that the desorption peak of $Cu_{0.50}$-MOR was obvious,

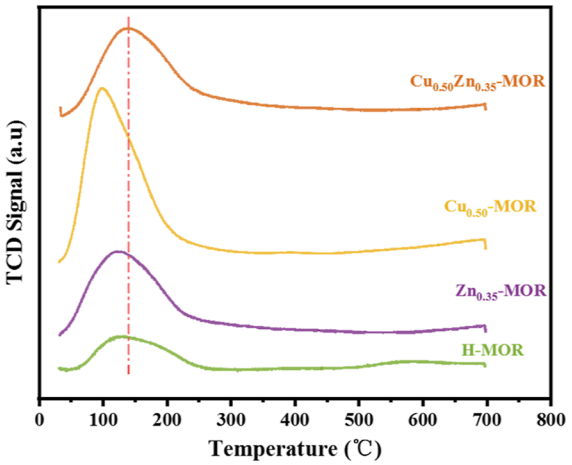

Figure 4. CH_4-TPD profiles for H-MOR $Cu_{0.50}$-MOR, $Zn_{0.35}$-MOR, and $Cu_{0.50}Zn_{0.35}$-MOR.

and the desorption peaks of bare H-MOR, $Zn_{0.35}$-MOR, and $Cu_{0.50}Zn_{0.35}$-MOR were all more moderate, among which the desorption peak of bare H-MOR was the smallest, indicating that the Cu species might be more favorable to enhance methane adsorption. However, the $Cu_{0.50}$-MOR catalyst exhibited the lowest desorption temperature, while the Zn-containing zeolite samples shifted to higher temperatures, suggesting that the presence of Zn may enhance the adsorption strength of methane on the catalyst. Although the results show that $Cu_{0.50}Zn_{0.35}$-MOR did not adsorb more methane than $Cu_{0.50}$-MOR, considering that the addition of Zn in the performance test results did enhance the methanol yield (shown below), we speculate that the intensity of methane adsorption during the reaction is a more important indicator than the temperature. These results indicated that the adsorption intensity of $Cu_{0.50}Zn_{0.35}$-MOR on methane was greater, which revealed that Zn not only promoted the dispersion of Cu but also enhanced the adsorption intensity of methane.

Solid-state ^{27}Al MAS NMR spectroscopy was one of the main characterization techniques for aluminosilicate molecular sieves, which provided a method to study the coordination of aluminum sites. The ^{27}Al MAS NMR spectra are displayed in Figure 5. The percentages of tetrahedrally coordinated FAl and

https://doi.org/10.1021/acsomega.3c02388
ACS Omega 2023, 8, 27179−27189

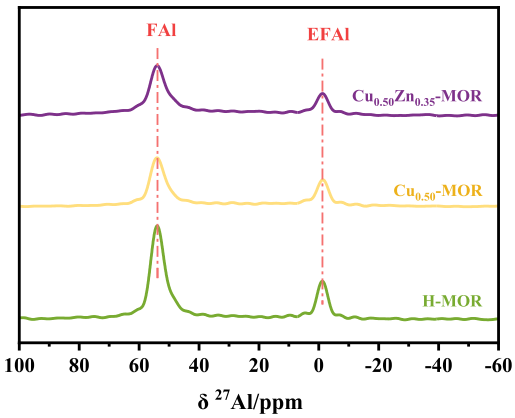

Figure 5. ^{27}Al MAS NMR spectra for the H-MOR, $Cu_{0.50}$-MOR, and $Cu_{0.50}Zn_{0.35}$-MOR catalysts.

octahedrally coordinated EFAl content were calculated by integrating each peak area in the catalyst and are summarized in Table 2. As reported in previous studies, the peak at 53.7 ppm was considered a tetrahedrally coordinated FAl peak, while the peak at 0 ppm was arranged as an octahedrally coordinated EFAl peak.[26,34,46,47] Both peaks were present in the bare H-MOR and modified catalysts, indicating that the impregnation and calcination did not change the tetrahedral and octahedral positions and the basic skeleton of aluminum. In addition, all modified H-MOR catalysts showed varying degrees of FAl and EFAl peak intensities, and the degree of variation was the largest for the Cu catalyst. As shown in Table 2, the amount of FAl on the $Cu_{0.50}$-MOR dramatically declined from the initial 77−69%, while it dropped to 72% on the $Cu_{0.50}Zn_{0.35}$-MOR. Although the FAl values all decreased after metal loading, the least amount of decrease was observed on the $Cu_{0.50}Zn_{0.35}$-MOR catalyst, indicating a lighter dealumination. Furthermore, the amount of EFAl in H-MOR, $Cu_{0.50}$-MOR, and $Cu_{0.50}Zn_{0.35}$-MOR were 23, 31, and 28%, respectively, indicating that the amount of EFAl on the catalysts all increased to different degrees after modification and the increase on $Cu_{0.50}Zn_{0.35}$-MOR was the least. Tetrahedrally coordinated FAl in zeolite can generate acid sites to anchor active sites.[46] Dyballa et al. proposed that the presence of EFAl during catalyst preparation might block the mordenite pores, which would prevent the uniform distribution of copper in the framework.[34] Therefore, the results indicated that the introduction of Zn promoted the distribution of Cu in the zeolite by reducing the production of EFAl. Furthermore, this further explained the trend of BET surface area change in the above section. The reason for the significant decrease in BET surface area for $Cu_{0.50}$-MOR was that, in addition to the metal particles, the large amount of EFAl production also caused the clogging of the zeolite itself. Correspondingly, less EFAl generation on the $Cu_{0.50}Zn_{0.35}$-MOR resulted in less pore blockage and thus less BET surface area loss.

Table 2. Percentage of FAl and EFAl Content on Each Catalyst

samples	FAl (%)	EFAl (%)
H-MOR	77	23
$Cu_{0.50}$-MOR	69	31
$Cu_{0.50}Zn_{0.35}$-MOR	72	28

The above NMR analysis indicated that Zn effected the change of Al species, but we cannot exclude that there was also an interaction between Cu and Zn. Therefore, additional characterization will be needed, as shown below, to prove whether or not there was an interaction between Cu and Zn.

To further investigate the interaction between Cu and Zn, we subsequently performed H_2 temperature-programmed reduction (H_2-TPR) studies on various catalysts, as shown in Figure 6. Compared with H-MOR, the H_2-TPR profiles for $Cu_{0.50}$-MOR and $Cu_{0.50}Zn_{0.35}$-MOR catalysts displayed a same broad reduction peak at 200 °C approximately. Low-temperature reduction peaks at about 200 °C generally were assigned to the reduction of the most accessible Cu sites on the external surface and in the largest cage of zeolite.[25,44,48−50] Theoretically, Zn was not reduced by hydrogen at least up to 900 °C.[25,51] The samples without copper showed no peak as well, which was consistent with the results reported. Most importantly, the introduction of Zn significantly shifted the reduction peak of $Cu_{0.50}Zn_{0.35}$-MOR to a higher temperature, indicating that there was indeed an interaction between Zn and Cu in this catalyst.

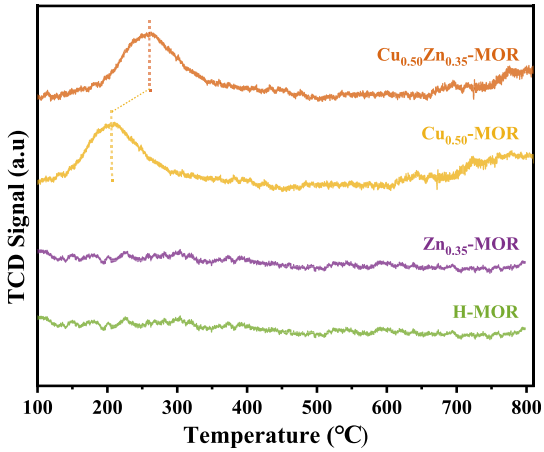

Figure 6. H_2-TPR profiles for H-MOR $Cu_{0.50}$-MOR, $Zn_{0.35}$-MOR, and $Cu_{0.50}Zn_{0.35}$-MOR.

Inspired by the results of ^{27}Al MAS NMR spectroscopy and H_2-TPR, XPS studies of the CuZn−MOR catalysts were carried out to obtain more direct information on the oxidation and surface chemical states of copper and zinc. The XPS core-level spectra of O 1s, Cu 2p, and Zn 2p are presented in Figure 7a,b separately, while the results of fitting the photoelectric emission peaks of the Cu $2p_{3/2}$ and Zn $2p_{3/2}$ catalysts were summarized in Table 3. The O 1s core-level spectra (Figure S5) for the $Zn_{0.35}$-MOR, $Cu_{0.50}$-MOR, and $Cu_{0.50}Zn_{0.35}$-MOR

Table 3. Fitting Results of the Photoemission Peaks for Cu $2p_{3/2}$ and Zn $2p_{3/2}$[a]

	Cu $2p_{3/2}$ (%)		Zn $2p_{3/2}$ (%)	
Samples	933.6 eV	936.4 eV	1022.2 eV	1024.2 eV
$Cu_{0.50}$-MOR	60	40	n.a.	n.a.
$Zn_{0.35}$-MOR	n.a.	n.a.	55	45
$Cu_{0.50}$ $Zn_{0.35}$-MOR	55	45	41	59

[a]n.a. Not available.

https://doi.org/10.1021/acsomega.3c02388
ACS Omega 2023, 8, 27179−27189

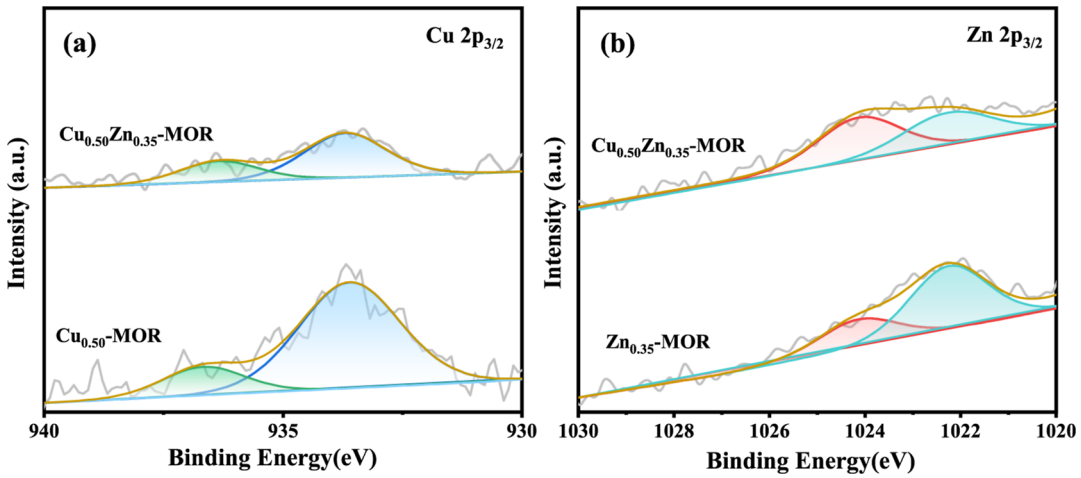

Figure 7. (a) Cu 2p and (b) Zn 2p core-level X-ray photoelectron spectra.

catalysts revealed only one type of oxygen species with binding energy (B.E.) of 533.4 eV, corresponding to the framework oxygen.[23,26,41]

The XPS core-level spectra of Cu 2p of $Cu_{0.50}$-MOR and $Cu_{0.50}Zn_{0.35}$-MOR catalysts are illustrated in Figure 7a. The oxidation state of copper in the active site of copper zeolite was mainly divalent but existed in various forms.[21,23,26,41,49] The fitting of the Cu $2p_{3/2}$ spectra for all catalysts exhibited two different peaks at 933.6 and 936.4 eV, which correspond to cupric oxides and Cu^{2+} species bound to zeolite framework oxygen [e.g., Cu−OH^+, mono, and bis (μ-oxo) dicopper and tricopper sites], respectively.[21] Yu et al. studied the surface structures of $CuO/MoO_3/CeO_2$ and proved by infrared spectroscopy that the presence of cupric oxides would decrease the Brønsted acid sites in the catalyst.[52] Also, Sushkevich et al. demonstrated that the presence of Brønsted acid sites on copper zeolites was more favorable for the oxidation of methane to methanol.[53] Therefore, it can be seen from Table 3 that the amount of divalent Cu oxides (933.6 eV) decreases from 60 to 55% with the introduction of Zn, in contrast to the increase in the amount of Cu species bound to the zeolite extra framework (936.4 eV) from 40 to 45%. This trend demonstrated that the introduction of Zn did indeed enhance the production of active sites (936.4 eV).

The Zn 2p XPS core-level spectra of $Cu_{0.50}$-MOR and $Cu_{0.50}Zn_{0.35}$-MOR catalysts are illustrated in Figure 7b. The B.E. peaks were around 1022.2 and 1024.2 eV, which were mainly composed of −O−Zn−OH species and Zn^{2+} cations in the cation exchange sites, respectively.[54,55] The −O−Zn−OH species (1022.2 eV) were considered to be precursors of small ZnO clusters, while Zn^{2+} cations in the cation exchange sites (1024.2 eV) indicated the presence of the zinc species having tighter interaction with the parent zeolite framework.[49,56] Combined with the fitted XPS spectra and Table 3, it was evident that the Cu−Zn interaction increases the amount of Zn^{2+} cations in the cation exchange sites (1024.2 eV) species from 45 to 59% compared to $Zn_{0.35}$-MOR, while the amount of the −O−Zn−OH species (1022.2 eV), i.e., ZnO precursor decreases from 55 to 41%. This phenomenon indicated that the dispersion of Zn on the bimetallic $Cu_{0.50}Zn_{0.35}$-MOR catalyst was better compared to the monometallic $Zn_{0.35}$-MOR catalyst.

Comprehensive results of the above analysis revealed that when monometallic Cu or Zn modified mordenite, more EFAl will be generated to hinder the distribution of the metals, resulting in their presence mostly as corresponding metal oxides on the zeolites. In contrast, when bimetallic Cu and Zn co-modified mordenite, the interaction between the two metals would degrade the formation of EFAl and make each other highly dispersed in the zeolite framework.

Subsequently, DR UV−Vis spectroscopy was used to study the electronic states of Cu and Zn in the catalysts to further confirm the above results. In addition, the normalized DR UV−Vis spectra of the various catalysts are depicted in Figure 8. Conspicuously, the Cu-containing samples all exhibited a

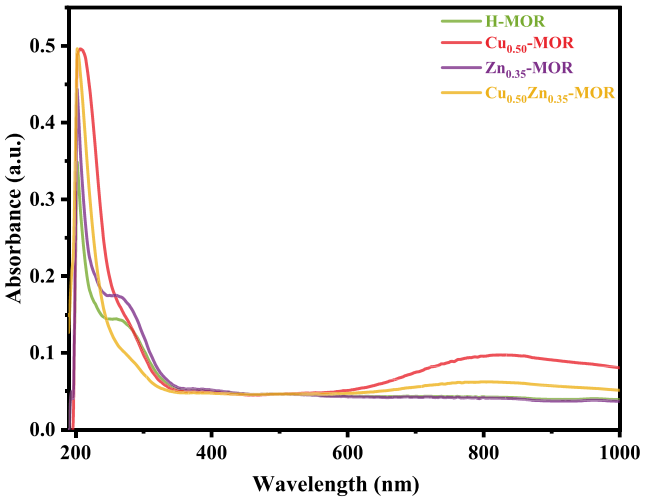

Figure 8. The normalized DR UV−Vis spectra for H-MOR $Cu_{0.50}$-MOR, $Zn_{0.35}$-MOR, and $Cu_{0.50}Zn_{0.35}$-MOR.

broad peak in the absorption band above 600 nm, which can be attributed to the d−d electron transitions of Cu^{2+} in octahedrally coordinated CuO particles.[36,57,58] Also, the intensity of this peak was markedly decreased on the $Cu_{0.50}Zn_{0.35}$-MOR catalyst, suggesting a dramatic diminution in the number of cupric oxides. Since the DR UV−Vis spectrum of a species was closely correlated with its electronic state, the change in the Cu species above 600 nm here must indicate that the introduction of Zn did change the electronic state of Cu. Furthermore, the weakened signal of the CuO on the $Cu_{0.50}Zn_{0.35}$-MOR catalyst suggested that more Cu could

https://doi.org/10.1021/acsomega.3c02388
ACS Omega 2023, 8, 27179−27189

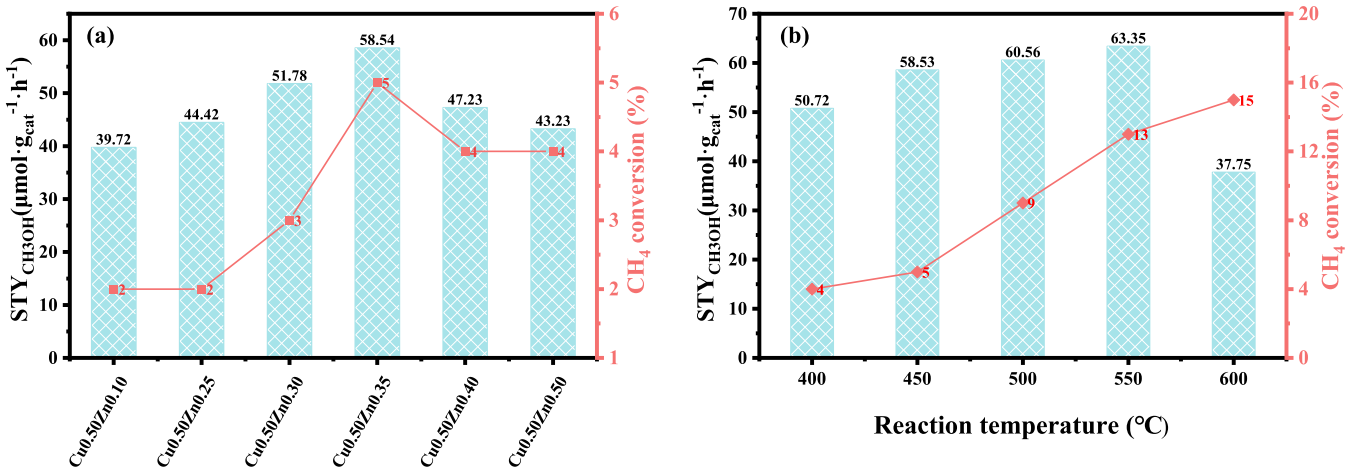

Figure 9. Effect of the methanol yield and methane conversion of (a) Zn loading over the relevant catalysts and (b) temperature over the $Cu_{0.50}Zn_{0.35}$-MOR catalyst. Reaction conditions: 50 mg catalyst, 16.67 sccm of 15% CH_4, 8.33 sccm of 21% O_2, T = 450 °C, water inflow = 1 μL·min^{-1}, 2 h.

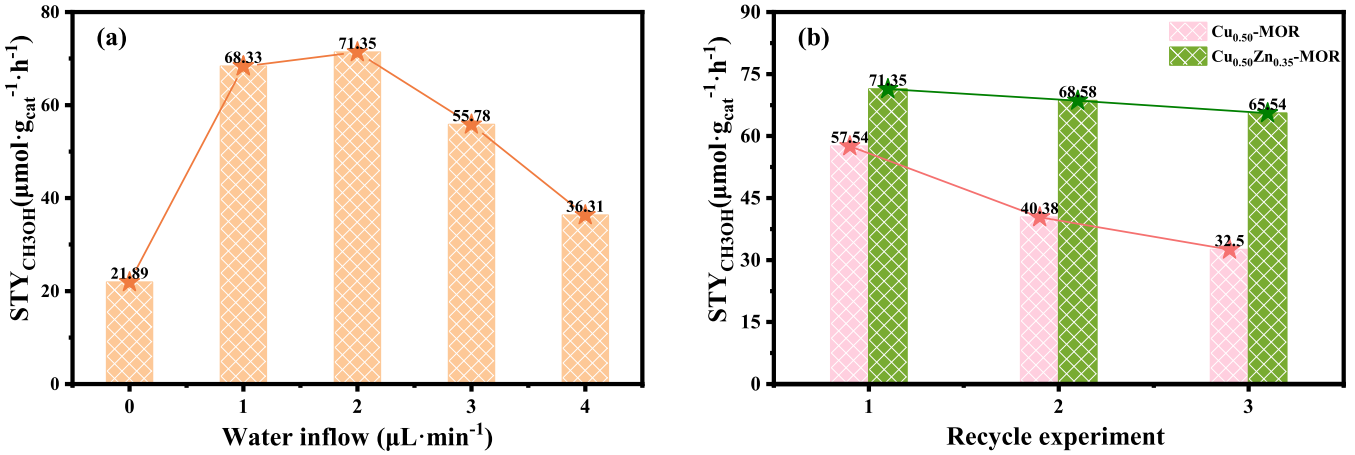

Figure 10. (a) Water inflow on methanol yield over the $Cu_{0.50}Zn_{0.35}$-MOR catalyst. Reaction conditions: 50 mg catalyst, 20 sccm of 15% CH_4, 10 sccm of 21% O_2, T = 550 °C, 2 h. (b) Recycle stability test over $Cu_{0.50}$-MOR and $Cu_{0.50}Zn_{0.35}$-MOR catalysts. Reaction conditions: 50 mg catalyst, 20 sccm of 15% CH_4, 10 sccm of 21% O_2, T = 550 °C, water inflow = 2 μL·min^{-1}, 2 h.

form other Cu species. These further corroborate the results of our analysis characterized above.

3.3. Catalyst Performance. First of all, we studied the effect of copper/zinc loading on the methanol space-time yield (STY_{CH_3OH}) and methane conversion under gas-phase conditions, and the results are shown in Table S1 and Figure 9a. Table S1 showed the presence of only trace amounts of methanol over H-MOR and copper-free catalysts. When Cu loading increased from 0.10 to 2.00 wt %, CH_4 conversion showed a continuously increasing trend, while methanol yield exhibited a volcanic curve, reaching a maximum of 39.52 μmol·g^{-1}·h^{-1} at 0.50 wt % and then gradually decreasing. The TEM, XPS, and DR UV−Vis results above demonstrated that the copper in Cu-MOR was more inclined to form copper oxide, which was not favorable to improving the methanol yield. On the other hand, the amount of zinc loading in the catalyst also had a significant effect on the reaction. As shown in Figure 9a, methane conversion and methanol yield were significantly improved after the introduction of zinc. When the mass fraction of zinc in the catalyst was gradually increased from 0.10 to 0.50 wt %, methanol yield and methane conversion maintained a consistent volcano curve trend, which reached a maximum of 58.54 μmol·g^{-1}·h^{-1} at 0.35 wt % and then decreased. Based on the analysis above, we speculated that a moderate amount of Zn could improve the distribution of Cu and favor the formation of active sites to enhance methanol yields, while an excess of Zn would have the opposite effect. Because the $Cu_{0.50}Zn_{0.35}$-MOR catalyst maintains the best activity under the same condition, we then altered the detailed parameters to obtain the optimal reaction conditions.

Figure 9b showed the effect of reaction temperature over the $Cu_{0.50}Zn_{0.35}$-MOR catalyst. As the temperature increased from 400 to 600 °C, the CH_4 conversion showed a continuously increasing trend, while the methanol yield presented a volcano curve with a maximum value of 63.35 μmol·g^{-1}·h^{-1} at 550 °C, and then dramatically decreased at 600 °C. Since methane has very low activity, it is easily over-oxidized when the first C−H bond is activated.[19,20] Therefore, at the higher reaction temperature, over-oxidation reactions may occur on the catalyst. The selectivity of CO_2 in this temperature interval showed a trend similar to that of the methane conversion (Figure S7), demonstrating that a very high temperature would cause severe over-oxidation, which well explained the sharp drop in methanol yield at 600 °C. Since we obtained the best

https://doi.org/10.1021/acsomega.3c02388
ACS Omega 2023, 8, 27179−27189

methanol yield at 550 °C, that temperature point was chosen as the optimal reaction temperature in the next study.

The effect of space velocity and the ratio of methane to oxygen was examined and is listed in the Supporting Information. As shown in Figure S8, the methanol yield decreased markedly in the absence of oxygen or at low oxygen content, which indicated that oxygen plays a crucial role in this reaction system. The results demonstrated that the optimized molar ratio of methane to oxygen in the reaction gas was 2:1 for the best reaction conditions. Figure S9 suggested that an appropriate increase of the space velocity in the reaction system was beneficial for improving the methanol yield, but a very high reaction space velocity would lower the contact time between the reactants and the catalyst and thus decrease the methanol yield. The optimized reaction air velocity was 36,000 $mL{\cdot}g^{-1}{\cdot}h^{-1}$. Figure 10a showed that the methanol yield was only 21.89 $\mu mol{\cdot}g^{-1}{\cdot}h^{-1}$ in the absence of steam, and increased remarkably to 71.35 $\mu mol{\cdot}g^{-1}{\cdot}h^{-1}$ when the water intake was increased to 2 $\mu L{\cdot}min^{-1}$. The subsequent continuous increase in water intake was detrimental to the methanol yield, due to the impeded contact of the reactants with the active site.

Cyclic experiments for the $Cu_{0.50}$-MOR and $Cu_{0.50}Zn_{0.35}$-MOR catalysts were carried out to demonstrate their applicability. Figure 10b showed that a significant decrease was observed in the activity of the $Cu_{0.50}$-MOR catalyst after three cycles, resulting in a decline in the yield of methanol from 57.54 to 32.50 $\mu mol{\cdot}g^{-1}{\cdot}h^{-1}$. In contrast, the introduction of Zn enhanced and improved the activity and stability, with only a slight decrease in the methanol yield from 71.35 to 65.54 $\mu mol{\cdot}g^{-1}{\cdot}h^{-1}$. The SEM results (Figure S3) revealed that some collapse was discovered in the $Cu_{0.50}$-MOR and $Cu_{0.50}Zn_{0.35}$-MOR catalysts after three repeated cycles, which led to a decrease in catalyst activity. Furthermore, in the TEM (Figure 1) images of the catalysts after three cycles, it could be seen that the decline in activity could be due to the formation of metal sintering agglomerates caused by multiple heating and cooling treatments in the cycling reaction. This result also well explains why $Cu_{0.50}Zn_{0.35}$-MOR has good repeatability. This further confirms that the introduction of Zn in the present work does enhance the dispersion of Cu on zeolite, thus improving the activity and stability. To further evaluate the thermodynamic stability of the $Cu_{0.50}Zn_{0.35}$-MOR catalyst, the effect of reaction time was examined, as shown in Figure S10. The results showed that the methanol yield remained stable as the reaction time increased from 1 to 5 h, which also reflected the good hydrothermal stability of the $Cu_{0.50}Zn_{0.35}$-MOR catalyst.

Numerous studies have also proved that various Cu−oxo complexes (including monomers, dimers, and trimers) were considered active sites for the reaction of methane to methanol on Cu−zeolite.[7,10,32,33,59] In addition, these copper species were coordinated to oxygen atoms bound to aluminum ions in the zeolite framework.[21] Interestingly, although there were no signs of Cu-dimer sites from our CuZn−MOR catalyst in the DR UV−Vis spectrum (Figure 8), XPS showed that the main active site was derived from Cu^{2+} species bound to the zeolite framework oxygen. According to published data, the absorption band appears around 450 nm (Cu-dimer) in the DR UV−Vis spectrum of Cu-based zeolite after activation in flowing O_2.[32,60,61] In this context, it was reasonable for us to speculate on the possible reaction mechanism of methane to methanol using Cu-dimer species as the active sites. At first, CH_4 was adsorbed and oxidized to $[Cu{-}CH_3]$ on the Cu-dimer species.[13] Then, it came into contact with OH dissociated by water molecules to form methanol.[32] The role of water in the methane to methanol reaction was to promote oxidation and extract the product.[13,32,62,63] Therefore, when methanol was extracted and removed, oxygen was released, leading to regeneration of the site. Specifically, the formation of Cu-dimer sites by oxidation signaled the beginning of the reaction. CH_4 then was adsorbed on Cu upon contact with the active site Cu-dimer and broke the C−H bond to form the $[Cu{-}CH_3]$ structure. Afterward, the OH formed by the dissociation of H_2O molecules interacted with $[Cu{-}CH_3]$ to form $[Cu{-}CH_3OH]$. CH_3OH was immediately desorbed from the active site. Finally, the active site was regenerated by O_2, at which point the reaction process was completed.

4. CONCLUSIONS

In summary, using a simple impregnation method, we prepared low-loading Cu and Zn bimetallic co-modified H-MOR zeolite catalysts for the direct oxidation of low-concentration methane to methanol. According to the catalyst performance test results, the main active species originated from copper rather than from zinc. Compared with $Cu_{0.50}$-MOR, $Cu_{0.50}Zn_{0.35}$-MOR exhibited better activity after three cycle test experiments. In addition, the results of SEM, TEM, XRD, and BET analyses confirmed that the modification of Cu and Zn did not change the morphology and structure of the pristine H-MOR. In addition, the combination of ^{27}Al MAS NMR, and XPS characterization results demonstrated that the introduction of Zn mainly enhanced the distribution of Cu on the mordenite framework by reducing the production of EFAl, thus promoting the generation of active sites. Furthermore, the CH_4-TPD results supported that the interaction between Zn and Cu can enhance the adsorption of methane, which also facilitates the reaction.

■ ASSOCIATED CONTENT

Supporting Information

The Supporting Information is available free of charge at https://pubs.acs.org/doi/10.1021/acsomega.3c02388.

Characterization parameters; experimental equipment diagram; SEM images; TEM−EDS elemental mapping; the O 1s core-level spectra; ^1H NMR; and gas product selectivity, activity test parameters, and stability test results (PDF)

■ AUTHOR INFORMATION

Corresponding Author

Wenzhi Li − *Laboratory of Basic Research in Biomass Conversion and Utilization, Department of Thermal Science and Energy Engineering, University of Science and Technology of China, Hefei 230026, China;* orcid.org/0000-0002-7082-5839; Email: liwenzhi@ustc.edu.cn

Authors

Yan Fu − *School of Earth and Environment, Anhui University of Science and Technology, Huainan 232001, China*

Cunshuo Li − *Laboratory of Basic Research in Biomass Conversion and Utilization, Department of Thermal Science and Energy Engineering, University of Science and Technology of China, Hefei 230026, China*

Shengxin An − *School of Earth and Environment, Anhui University of Science and Technology, Huainan 232001, China*

Liang Yuan − *National & Local Joint Engineering Research Center of Precision Coal Mining, Anhui University of Science and Technology, Huainan 232001, China*

Complete contact information is available at: https://pubs.acs.org/10.1021/acsomega.3c02388

Author Contributions

Yan Fu and Wenzhi Li: conceptualization and methodology; Yan Fu: writing—original draft; Yan Fu, Wenzhi Li, and Cunshuo Li: writing—review and editing; Wenzhi Li and Liang Yuan: funding acquisition; and Yan Fu and Shengxin An: experiments and data analysis.

Notes

The authors declare no competing financial interest.

All relevant data are available from the authors on reasonable request.

■ ACKNOWLEDGMENTS

This work was supported by the Major Science and Technology Projects of Anhui Province (202003a05020022), the Graduate Innovation Fund Project of Anhui University of Science and Technology (2021CX2006), the Institute of Energy, Hefei Comprehensive National Science Center under grant no. 21KZS219, and the Key Research and Development Projects in Anhui Province (202004a06020053).

■ REFERENCES

(1) Sun, X.; Chen, X.; Fu, C.; Yu, Q.; Zheng, X.-S.; Fang, F.; Liu, Y.; Zhu, J.; Zhang, W.; Huang, W. Molecular oxygen enhances H_2O_2 utilization for the photocatalytic conversion of methane to liquid-phase oxygenates. *Nat. Commun.* **2022**, *13*, 6677.

(2) Jiang, Y.; Li, W.; Chen, K.; Zhang, X.; Shen, C.; Yuan, L. A rod-like Co_3O_4 with high efficiency and large specific surface area for lean methane catalytic oxidation. *Mol. Catal.* **2022**, *522*, 112229.

(3) Wu, M.; Li, W.; Zhang, X.; Xue, F.; Yang, T.; Yuan, L. Penta-coordinated Al^{3+} Stabilized Defect-Rich Ceria on Al_2O_3 Supported Palladium Catalysts for Lean Methane Oxidation. *ChemCatChem* **2021**, *13*, 3490−3500.

(4) Tao, L.; Lee, I.; Khare, R.; Jentys, A.; Fulton, J. L.; Sanchez-Sanchez, M.; Lercher, J. A. Speciation of Cu-Oxo Clusters in Ferrierite for Selective Oxidation of Methane to Methanol. *Chem. Mater.* **2022**, *34*, 4355−4363.

(5) Chen, K.; Li, W.; Guo, G.; Zhu, C.; Wu, W.; Yuan, L. Nickel Hydroxide Nanosheets Prepared by a Direct Manual Grinding Strategy for High-Efficiency Catalytic Combustion of Methane. *ACS Omega* **2022**, *7*, 8536−8546.

(6) Tomkins, P.; Ranocchiari, M.; van Bokhoven, J. A. Direct Conversion of Methane to Methanol under Mild Conditions over Cu-Zeolites and beyond. *Acc. Chem. Res.* **2017**, *50*, 418−425.

(7) Fang, Z.; Huang, M.; Liu, B.; Jiang, F.; Xu, Y.; Liu, X. Identifying the crucial role of water and chloride for efficient mild oxidation of methane to methanol over a $[Cu_2(\mu\text{-}O)]^{2+}$-ZSM-5 catalyst. *J. Catal.* **2022**, *405*, 1−14.

(8) Chen, K.; Li, W.; Li, X.; Ogunbiyi, A. T.; Yuan, L. Irregularly Shaped NiO Nanostructures for Catalytic Lean Methane Combustion. *ACS Appl. Nano Mater.* **2021**, *4*, 5404−5412.

(9) Li, C.; Li, W.; Chen, K.; Ogunbiyi, A. T.; Zhou, Z.; Xue, F.; Yuan, L. Palladium Nanoparticles Supported on Surface-Modified Metal Oxides for Catalytic Oxidation of Lean Methane. *ACS Appl. Nano Mater.* **2020**, *3*, 12130−12138.

(10) Tang, X.; Wang, L.; Yang, B.; Fei, C.; Yao, T.; Liu, W.; Lou, Y.; Dai, Q.; Cai, Y.; Cao, X.-M.; Zhan, W.; Guo, Y.; Gong, X.-Q.; Guo, Y. Direct oxidation of methane to oxygenates on supported single Cu atom catalyst. *Appl. Catal. B Environ.* **2021**, *285*, 119827.

(11) Yang, L.; Huang, J.; Ma, R.; You, R.; Zeng, H.; Rui, Z. Metal-Organic Framework-Derived IrO_2/CuO Catalyst for Selective Oxidation of Methane to Methanol. *ACS Energy Lett.* **2019**, *4*, 2945−2951.

(12) Xi, Y.; Heyden, A. Direct Oxidation of Methane to Methanol Enabled by Electronic Atomic Monolayer−Metal Support Interaction. *ACS Catal.* **2019**, *9*, 6073−6079.

(13) Sun, L.; Wang, Y.; Wang, C.; Xie, Z.; Guan, N.; Li, L. Water-involved methane-selective catalytic oxidation by dioxygen over copper zeolites. *Chem* **2021**, *7*, 1557−1568.

(14) Sushkevich, V. L.; Palagin, D.; Ranocchiari, M.; van Bokhoven, J. A. Selective anaerobic oxidation of methane enables direct synthesis of methanol. *Science* **2017**, *356*, 523−527.

(15) Wu, W.; Li, W.; Wu, M.; Zhang, H.; Zhu, C.; Jiang, Y. Direct oxidation of methane to methanol using $CuMoO_4$. *RSC Adv.* **2023**, *13*, 5393−5404.

(16) Periana, R. A.; Taube, D. J.; Gamble, S.; Taube, H.; Satoh, T.; Fujii, H. Platinum Catalysts for the High-Yield Oxidation of Methane to a Methanol Derivative. *Science* **1998**, *280*, 560−564.

(17) Xi, Z.; Zhou, B.; Yu, Y.; Jiang, B.; Liao, Z.; Wang, J.; Huang, Z.; Yang, Y.; Sun, J.; Yang, Y. Enhancing low-temperature methane conversion on Zn/ZSM-5 in the presence of methanol by regulating the methanol-to-aromatics reaction pathway. *Catal. Sci. Technol.* **2020**, *10*, 6161−6172.

(18) Li, C.; Tang, B.; Ogunbiyi, A. T.; Tang, S.; Li, W.; Lu, Q.; Yuan, L. The effects of facet-dependent palladium-titania interactions on the activity of Pd/Rutile catalysts for lean methane oxidation. *Mol. Catal.* **2022**, *528*, 112475.

(19) Ravi, M.; Ranocchiari, M.; van Bokhoven, J. A. The Direct Catalytic Oxidation of Methane to Methanol-A Critical Assessment. *Angew. Chem., Int. Ed.* **2017**, *56*, 16464−16483.

(20) Olivos-Suarez, A. I.; Szécsényi, À.; Hensen, E. J. M.; Ruiz-Martinez, J.; Pidko, E. A.; Gascon, J. Strategies for the Direct Catalytic Valorization of Methane Using Heterogeneous Catalysis: Challenges and Opportunities. *ACS Catal.* **2016**, *6*, 2965−2981.

(21) Artiglia, L.; Sushkevich, V. L.; Palagin, D.; Knorpp, A. J.; Roy, K.; van Bokhoven, J. A. In Situ X-ray Photoelectron Spectroscopy Detects Multiple Active Sites Involved in the Selective Anaerobic Oxidation of Methane in Copper-Exchanged Zeolites. *ACS Catal.* **2019**, *9*, 6728−6737.

(22) Liu, Z.; Huang, E.; Orozco, I.; Liao, W.; Palomino, R. M.; Rui, N.; Duchon, T.; Nemšák, S.; Grinter, D. C.; Mahapatra, M.; Liu, P.; Rodriguez, J. A.; Senanayake, S. D. Water-promoted interfacial pathways in methane oxidation to methanol on a CeO2-Cu2O catalyst. *Science* **2020**, *368*, 513−517.

(23) Priya, S. S.; Selvakannan, P. R.; Chary, K. V. R.; Kantam, M. L.; Bhargava, S. K. Solvent-free microwave-assisted synthesis of solketal from glycerol using transition metal ions promoted mordenite solid acid catalysts. *Mol. Catal.* **2017**, *434*, 184−193.

(24) Asuquo, R. A.; Edermirth, G.; Lercher, J. A. n -Butane Isomerization over Acidic Mordenite. *J. Catal.* **1995**, *155*, 376−382.

(25) Reule, A. A. C.; Prasad, V.; Semagina, N. Effect of Cu and Zn ion-exchange locations on mordenite performance in dimethyl ether carbonylation. *Microporous Mesoporous Mater.* **2018**, *263*, 220−230.

(26) Priya, S. S.; Bhanuchander, P.; Kumar, V. P.; Bhargava, S. K.; Chary, K. V. R. Activity and Selectivity of Platinum−Copper Bimetallic Catalysts Supported on Mordenite for Glycerol Hydrogenolysis to 1,3-Propanediol. *Ind. Eng. Chem. Res.* **2016**, *55*, 4461−4472.

(27) Li, C.; Tang, B.; Li, W.; Lu, Q.; Yuan, L. Palladium Nanoparticles Encapsulated in Surface-Defected SBA-15 for Lean Methane Oxidation. *ACS Appl. Nano Mater.* **2022**, *5*, 13055−13068.

(28) Wang, L.; Sang, S.; Meng, S.; Zhang, Y.; Qi, Y.; Liu, Z. Direct synthesis of Zn-ZSM-5 with novel morphology. *Mater. Lett.* **2007**, *61*, 1675−1678.

(29) Snyder, B. E. R.; Vanelderen, P.; Schoonheydt, R. A.; Sels, B. F.; Solomon, E. I. Second-Sphere Effects on Methane Hydroxylation in Cu-Zeolites. *J. Am. Chem. Soc.* **2018**, *140*, 9236−9243.
(30) Pappas, D. K.; Borfecchia, E.; Dyballa, M.; Lomachenko, K. A.; Martini, A.; Berlier, G.; Arstad, B.; Lamberti, C.; Bordiga, S.; Olsbye, U.; Svelle, S.; Beato, P. Understanding and Optimizing the Performance of Cu-FER for The Direct CH_4 to CH_3OH Conversion. *ChemCatChem* **2018**, *11*, 621−627.
(31) Jeong, Y. R.; Jung, H.; Kang, J.; Han, J. W.; Park, E. D. Continuous Synthesis of Methanol from Methane and Steam over Copper-Mordenite. *ACS Catal.* **2021**, *11*, 1065−1070.
(32) Xu, R.; Liu, N.; Dai, C.; Li, Y.; Zhang, J.; Wu, B.; Yu, G.; Chen, B. H2O Built Proton Transfer Bridge Enhances Continuous Methane Oxidation to Methanol over Cu-BEA Zeolite. *Angew. Chem.* **2021**, *133*, 16770−16776.
(33) Sushkevich, V. L.; Palagin, D.; van Bokhoven, J. A. The Effect of the Active-Site Structure on the Activity of Copper Mordenite in the Aerobic and Anaerobic Conversion of Methane into Methanol. *Angew. Chem., Int. Ed.* **2018**, *57*, 8906−8910.
(34) Dyballa, M.; Pappas, D. K.; Kvande, K.; Borfecchia, E.; Arstad, B.; Beato, P.; Olsbye, U.; Svelle, S. On How Copper Mordenite Properties Govern the Framework Stability and Activity in the Methane-to-Methanol Conversion. *ACS Catal.* **2018**, *9*, 365−375.
(35) Hammond, C.; Forde, M. M.; AbRahim, M. H.; Thetford, A.; He, Q.; Jenkins, R. L.; Dimitratos, N.; Lopez-Sanchez, J. A.; Dummer, N. F.; Murphy, D. M.; Carley, A. F.; Taylor, S. H.; Willock, D. J.; Stangland, E. E.; Kang, J.; Hagen, H.; Kiely, C. J.; Hutchings, G. J. Direct Catalytic Conversion of Methane to Methanol in an Aqueous Medium by using Copper-Promoted Fe-ZSM-5. *Angew. Chem., Int. Ed.* **2012**, *51*, 5129−5133.
(36) Yu, T.; Li, Z.; Lin, L.; Chu, S.; Su, Y.; Song, W.; Wang, A.; Weckhuysen, B. M.; Luo, W. Highly Selective Oxidation of Methane into Methanol over Cu-Promoted Monomeric Fe/ZSM-5. *ACS Catal.* **2021**, *11*, 6684−6691.
(37) Yang, H.; Dang, Y.; Cui, X.; Bu, X.; Li, J.; Li, S.; Sun, Y.; Gao, P. Selective synthesis of olefins via CO_2 hydrogenation over transition-metal-doped iron-based catalysts. *Appl. Catal. B Environ.* **2023**, *321*, 122050.
(38) Wang, Y.; Wang, X.; Yan, Z.; Xu, C.; Zhang, W.; Ban, H.; Li, C. Activation reconstructing $CuZnO/SiO_2$ catalyst for CO_2 hydrogenation. *J. Catal.* **2022**, *412*, 10−20.
(39) Behrens, M.; Studt, F.; Kasatkin, I.; Kühl, S.; Hävecker, M.; Abild-Pedersen, F.; Zander, S.; Girgsdies, F.; Kurr, P.; Kniep, B.-L.; Tovar, M.; Fischer, R. W.; Nørskov, J. K.; Schlögl, R. The Active Site of Methanol Synthesis over $Cu/ZnO/Al_2O_3$ Industrial Catalysts. *Science* **2012**, *336*, 893−897.
(40) Zhang, Z.; Chen, X.; Kang, J.; Yu, Z.; Tian, J.; Gong, Z.; Jia, A.; You, R.; Qian, K.; He, S.; Teng, B.; Cui, Y.; Wang, Y.; Zhang, W.; Huang, W. The active sites of Cu−ZnO catalysts for water gas shift and CO hydrogenation reactions. *Nat. Commun.* **2021**, *12*, 4331.
(41) Wu, Y.; Zhang, H.; Yan, Y. High efficiency of phenol oxidation in a structured fixed bed over Cu-ZSM-5/PSSF prepared by ion-exchanged method. *Chem. Eng. J.* **2020**, *380*, 122466.
(42) Sakizci, M.; Tanriverdi, L. Ö. Influence of acid and heavy metal cation exchange treatments on methane adsorption properties of mordenite. *Turk. J. Chem.* **2015**, *39*, 970−983.
(43) Thommes, M. *Physisorption of gases, with special reference to the evaluation of surface area and pore size distribution (IUPAC Technical Report)*; Chemistry International The News Magazine of IUPAC, 2016; Vol *38*, p 25.
(44) Le, H. V.; Parishan, S.; Sagaltchik, A.; Göbel, C.; Schlesiger, C.; Malzer, W.; Trunschke, A.; Schomäcker, R.; Thomas, A. Solid-State Ion-Exchanged Cu/Mordenite Catalysts for the Direct Conversion of Methane to Methanol. *ACS Catal.* **2017**, *7*, 1403−1412.
(45) Bang, Y.; Han, S. J.; Yoo, J.; Choi, J. H.; Lee, J. K.; Song, J. H.; Lee, J.; Song, I. K. Hydrogen production by steam reforming of simulated liquefied natural gas (LNG) over nickel catalyst supported on mesoporous phosphorus-modified alumina xerogel. *Appl. Catal. B Environ.* **2014**, *148−149*, 269−280.
(46) Jiang, Y.; Huang, J.; Dai, W.; Hunger, M. Solid-state nuclear magnetic resonance investigations of the nature, property, and activity of acid sites on solid catalysts. *Solid State Nucl. Magn. Reson.* **2011**, *39*, 116−141.
(47) Zhou, L.; Li, S.; Su, Y.; Li, B.; Deng, F. Paramagnetic relaxation enhancement solid-state NMR studies of heterogeneous catalytic reaction over HY zeolite using natural abundance reactant. *Solid State Nucl. Magn. Reson.* **2015**, *66−67*, 29−32.
(48) Wang, Y.; Fan, L.; Xu, H.; Du, X.; Xiao, H.; Qian, J.; Zhu, Y.; Tu, X.; Wang, L. Insight into the synthesis of alcohols and acids in plasma-driven conversion of CO_2 and CH_4 over copper-based catalysts. *Appl. Catal. B Environ.* **2022**, *315*, 121583−121595.
(49) Chotigkrai, N.; Tannititam, P.; Piticharoenphun, S.; Triamnak, N.; Praserthdam, S.; Praserthdam, P. The effect of Zn doping on active Cu species and its location of Cu-exchanged mordenite for the stepwise oxidation of methane to methanol. *Korean J. Chem. Eng.* **2022**, *39*, 920−927.
(50) Armandi, M.; Andana, T.; Bensaid, S.; Piumetti, M.; Bonelli, B.; Pirone, R. Effect of the preparation technique of Cu-ZSM-5 catalysts on the isothermal oscillatory behavior of nitrous oxide decomposition. *Catal. Today* **2020**, *345*, 59−70.
(51) Biscardi, J. A.; Meitzner, G. D.; Iglesia, E. Structure and Density of Active Zn Species in Zn-H-ZSM5 Propane Aromatization Catalysts. *J. Catal.* **1998**, *179*, 192−202.
(52) Yu, W.; Zhu, J.; Qi, L.; Sun, C.; Gao, F.; Dong, L.; Chen, Y. Surface structure and catalytic properties of MoO_3/CeO_2 and $CuO/MoO_3/CeO_2$. *J. Colloid Interface Sci.* **2011**, *364*, 435−442.
(53) Sushkevich, V. L.; van Bokhoven, J. A. Effect of Brønsted acid sites on the direct conversion of methane into methanol over copper-exchanged mordenite. *Catal. Sci. Technol.* **2018**, *8*, 4141−4150.
(54) Tamiyakul, S.; Ubolcharoen, W.; Tungasmita, D. N.; Jongpatiwut, S. Conversion of glycerol to aromatic hydrocarbons over Zn-promoted HZSM-5 catalysts. *Catal. Today* **2015**, *256*, 325−335.
(55) Gabrienko, A. A.; Arzumanov, S. S.; Toktarev, A. V.; Danilova, I. G.; Prosvirin, I. P.; Kriventsov, V. V.; Zaikovskii, V. I.; Freude, D.; Stepanov, A. G. Different Efficiency of Zn^{2+} and ZnO Species for Methane Activation on Zn-Modified Zeolite. *ACS Catal.* **2017**, *7*, 1818−1830.
(56) Niu, X.; Gao, J.; Miao, Q.; Dong, M.; Wang, G.; Fan, W.; Qin, Z.; Wang, J. Influence of preparation method on the performance of Zn-containing HZSM-5 catalysts in methanol-to-aromatics. *Microporous Mesoporous Mater.* **2014**, *197*, 252−261.
(57) Ismagilov, Z. R.; Yashnik, S. A.; Anufrienko, V. F.; Larina, T. V.; Vasenin, N. T.; Bulgakov, N. N.; Vosel, S. V.; Tsykoza, L. T. Linear nanoscale clusters of CuO in Cu-ZSM-5 catalysts. *Appl. Surf. Sci.* **2004**, *226*, 88−93.
(58) Li, Y.; Deng, J.; Song, W.; Liu, J.; Zhao, Z.; Gao, M.; Wei, Y.; Zhao, L. Nature of Cu Species in Cu−SAPO-18 Catalyst for NH3−SCR: Combination of Experiments and DFT Calculations. *J. Phys. Chem. C* **2016**, *120*, 14669−14680.
(59) Grundner, S.; Markovits, M. A. C.; Li, G.; Tromp, M.; Pidko, E. A.; Hensen, E. J. M.; Jentys, A.; Sanchez-Sanchez, M.; Lercher, J. A. Single-site trinuclear copper oxygen clusters in mordenite for selective conversion of methane to methanol. *Nat. Commun.* **2015**, *6*, 7546.
(60) Vanelderen, P.; Snyder, B. E. R.; Tsai, M.-L.; Hadt, R. G.; Vancauwenbergh, J.; Coussens, O.; Schoonheydt, R. A.; Sels, B. F.; Solomon, E. I. Spectroscopic Definition of the Copper Active Sites in Mordenite: Selective Methane Oxidation. *J. Am. Chem. Soc.* **2015**, *137*, 6383−6392.
(61) Groothaert, M. H.; Smeets, P. J.; Sels, B. F.; Jacobs, P. A.; Schoonheydt, R. A. Selective Oxidation of Methane by the Bis(μ-oxo)dicopper Core Stabilized on ZSM-5 and Mordenite Zeolites. *J. Am. Chem. Soc.* **2005**, *127*, 1394−1395.
(62) Liu, Z.; Huang, E.; Orozco, I.; Liao, W.; Palomino, R. M.; Rui, N.; Duchoň, T.; Nemšák, S.; Grinter, D. C.; Mahapatra, M.; Liu, P.; Rodriguez, J. A.; Senanayake, S. D. Water-promoted interfacial pathways in methane oxidation to methanol on a CeO_2-Cu_2O catalyst. *Science* **2020**, *368*, 513−517.

https://doi.org/10.1021/acsomega.3c02388
ACS Omega 2023, 8, 27179−27189

(63) Imyen, T.; Znoutine, E.; Suttipat, D.; Iadrat, P.; Kidkhunthod, P.; Bureekaew, S.; Wattanakit, C. Methane Utilization to Methanol by a Hybrid Zeolite@Metal−Organic Framework. *ACS Appl. Mater. Interfaces* **2020**, *12*, 23812−23821.

https://doi.org/10.1021/acsomega.3c02388
ACS Omega 2023, 8, 27179−27189